





**Electrical switching of the light color reflected from a NiFe/IrMn mirror**M. V. Bakhmetiev <sup>1,2,3</sup>, A. I. Chernov <sup>2,4</sup>, A. B. Khutueva <sup>5</sup>, A. V. Sadovnikov,<sup>5,6</sup> and R. B. Morgunov <sup>1,2,3,\*</sup><sup>1</sup>*Federal Research Center of Problems of Chemical Physics and Medicinal Chemistry RAS, Chernogolovka 142432, Russia*<sup>2</sup>*Russian Quantum Center, 143025 Skolkovo, Russia*<sup>3</sup>*I.M. Sechenov First Moscow State Medical University, 119991 Moscow, Russia*<sup>4</sup>*Center for Photonics and 2D Materials, Moscow Institute of Physics and Technology, 14170 Dolgoprudny, Russia*<sup>5</sup>*Laboratory “Metamaterials,” Saratov State University, Saratov 410012, Russia*<sup>6</sup>*Laboratory of Spin-Orbitronics, Institute of High Technologies and Advanced Materials, Far Eastern Federal University, Vladivostok 690922, Russia*

(Received 18 August 2023; revised 24 November 2023; accepted 12 January 2024; published 26 January 2024)

A magnon-assisted electrically driven “mirror” with tuned frequency of the reflected light is created. The effect of in-plane electric current on asymmetry of Stokes–anti-Stokes Brillouin intensities in NiFe/IrMn exchange-biased patterned structures is found. Electric current directed along external magnetic field suppresses anti-Stokes component in Brillouin light-scattering spectra, while the opposite direction of current results in suppression of the Stokes component. We show that spin currents arising in the IrMn layer induce spin-orbit torque affecting uncompensated antiferromagnetic moments at the interface, rotate the antiferromagnetic moments, change bias field, and finally determine direction of dominating spin-wave propagation. The possibility of electric control of spin-wave direction and manipulation over Stokes and anti-Stokes intensities opens a way for design of electro-optical devices switching light frequency.

DOI: [10.1103/PhysRevB.109.024433](https://doi.org/10.1103/PhysRevB.109.024433)**I. INTRODUCTION**

Antiferromagnetic (AFM) spintronics devices significantly surpass ferromagnetic devices due to high density of elements and superfast switching of logic states [1–5]. The absence of macroscopic magnetization and terahertz spin dynamics give significant advantages to antiferromagnetic structures. Since magnetic field does not change magnetic order in antiferromagnets, the main instrument for magnetization control is spin-polarized electron current. Electric control over spin configuration in antiferromagnet has a great importance for realization of antiferromagnetic spintronics. Key strategy to create AFM logic elements is creation of interface AFM/HM of the antiferromagnet with a heavy transition metal (HM), where magnetization can be changed under electric field due to the Rashba-Edelstein effect [6–8] or spin Hall effect in the heavy nonmagnetic metal layer (Pt, Pd, etc.) [9–11]. Interaction of spin-polarized electrons with magnetic moments of crystal lattice ions through the spin-orbital coupling results in spin-orbital torque (SOT) affecting magnetization direction [12–15]. This effect is quite similar to the one described at interface FM/HM [12–15]. Spin-polarized current is investigated in antiferromagnets IrMn, PtMn, and MnN neighboring ferromagnets in metallic bilayer structures [16–18], as well as in structures with dielectric AFM layer NiO [19]. The reorientation of magnetic moments in an AFM under electric field or current demonstrates stable states into which the AFM spin system can switch under large enough current density.

The switching of the local magnetization in AFM depends on the domain structure, since the SOT induced by the current affects the motion of the domain walls. Since the magnetic moment of an antiferromagnet is small, and changes of magnetic properties under the action of a current are difficult to register, a cover ferromagnetic layer is used as an indicator film sensitive to magnetic transformations in AFM. The magnetic anisotropy, magnetization, and other properties of the FM layer can change significantly with variations in the magnetic ordering in the adjacent AFM layer under the action of the spin-polarized electric current [16–19].

Current-induced changes in the exchange bias in two-layer AFM/FM structures were reported in Ref. [16]. The authors of Ref. [16] found that the in-plane Hall resistance in NiFe/IrMn changes under the action of the current flowing in the plane of the structure and retains its value even after the current is turned off. It has been proven that SOT caused by the spin Hall effect in IrMn effectively reverses the direction of the exchange bias field. It was shown that SOT is not directly related to the ferromagnetic NiFe layer, but arises at the uncompensated magnetic moments of the antiferromagnet at the NiFe/IrMn interface, where the current stimulates the collective rotation of the magnetization of the exchange-coupled NiFe/IrMn bilayer. The crucial role of the interface is proved. Uncompensated spins in the antiferromagnetic layer transfer magnetization to the exchange coupled spins in ferromagnetic layer.

Since the exchange-bias field in bilayer structures affects the entire set of various properties associated with spin configurations at the interface, it can be expected that the response to exchange-bias switching by the spin-orbit torque of charge

\*spintronics2022@yandex.ru

carriers can also be a change in the Brillouin light-scattering (BLS) spectrum. The exchange-bias effect occurs as a result of the exchange coupling between adjacent ferromagnetic and antiferromagnetic layers cooled in a magnetic field from temperature above the Néel temperature [20]. It manifests itself as a shift of the hysteresis loop along the axis of the applied field, and is often described as in-plane unidirectional anisotropy. Although exchange-biased systems have been extensively studied, the microscopic origin of the exchange-bias effect is still unclear. Current models assume the formation of magnetic domains in the AFM layer [21].

It was shown in Refs. [22–24] that the exchange bias can significantly affect the BLS spectra. At least three mechanisms are known from the literature that can explain the effect of the exchange bias on the BLS spectra in NiFe/IrMn structures: (1) a change in the thermal population of magnonic energy levels, (2) the effect of the anisotropy field, leading to a shift of resonant frequencies in the BLS spectra, and (3) a change in the off-diagonal components of the spin operator  $S_x S_y$ , which arises due to the rotation of the magnetization vector in the ferromagnetic film. Thus, in Ref. [22], the anisotropy in Fe/FeF<sub>2</sub> bilayers with exchange bias was measured by the BLS method for spin waves in the Fe layer. This method, in which the ferromagnetic layer is always saturated, allows a direct and precise determination of the exchange-bias field.

Significant broadening of the BLS lines due to the presence of an antiferromagnet was reported in Ref. [23], where the change in the BLS spectra in the (110)-oriented NiFe/FeMn bilayer was interpreted as a change in the symmetry and contributions to the magnetic anisotropy under the action of the exchange bias. In Ref. [24], the origin of rotational anisotropy in NiFe/IrMn bilayers was investigated using magneto-optical magnetometry based on the Kerr effect, ferromagnetic resonance, and the BLS method. The dependence of magnon frequencies on the external magnetic field applied in the bilayer plane was measured by the BLS method. The rotational anisotropy associated with the presence of the exchange bias causes a frequency shift in the BLS spectra. It was demonstrated in Ref. [25] that an AFM can be used for highly efficient electrical manipulations of the magnetization in a FM layer. In Ref. [25], an antidamping torque acting on a NiFe ferromagnet was observed under in-plane current in IrMn antiferromagnetic layer.

In the IrMn antiferromagnet, the magnitude of the spin torque, which is characterized by the effective angle of the spin Hall effect, is much higher than SOT in heavy transition metals. Therefore, the object of our study was an IrMn antiferromagnet layer with a NiFe ferromagnet deposited below it. It was found that the SOT switching that occurs in the antiferromagnetic layer when an electric current is passed through it changes the exchange bias and the corresponding unidirectional anisotropy in the ferromagnet, which can be detected from the change in the spectra of spin waves recorded using Brillouin light scattering.

By using the BLS we reveal the influence of the exchange-bias variations caused by the action of SOT during the flow of current in an antiferromagnet IrMn and are able to control the propagation of the forward and backward spin waves in NiFe ferromagnet.

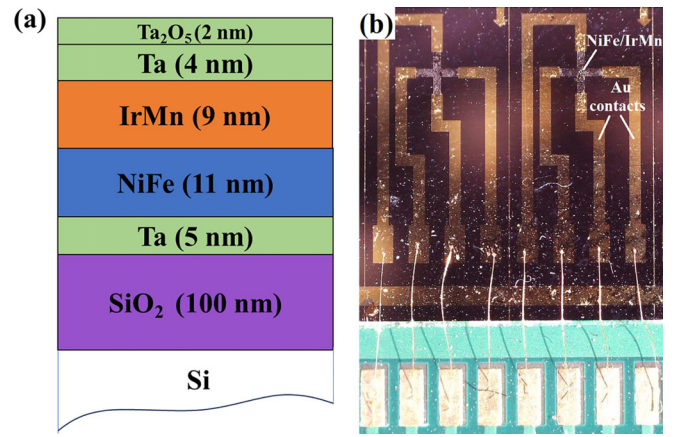


FIG. 1. (a) Sketch of the cross section of heterostructure, and (b) optical image of the contacts of the patterned sample. Arrows in the upper part of the photograph indicate the direction of the exchange-bias field and the corresponding unidirectional anisotropy fixed during deposition and cooling of the structure.

## II. EXPERIMENTAL TECHNIQUES AND SAMPLES

In the experiments, we used a Ta<sub>2</sub>O<sub>5</sub>(2 nm)/Ta(4 nm)/IrMn(9 nm)/NiFe(11 nm)/Ta(5 nm)/SiO<sub>2</sub>/Si multilayer heterostructure with in-plane anisotropy. The heterostructures were deposited by DC magnetron sputtering on a Si/SiO<sub>2</sub> substrate at room temperature with a thermally grown SiO<sub>2</sub> oxide layer 100 nm thick to prevent leakage of electric current, which affects the measurement accuracy. The base pressure in the main sputtering chamber was about  $2 \times 10^{-7}$  Torr. The operating pressure of argon was fixed at  $3 \times 10^{-3}$  Torr. The argon flow rate was maintained at 30 cm<sup>3</sup>/s. The rotation speed 10 rpm/min was kept constant during the deposition of the samples to create more uniform layers. The deposition rates of the Ta, IrMn, and NiFe layers were 0.05, 0.04, and 0.012 nm/s, respectively. The sample holder had a built-in magnet, generating magnetic field of 200 Oe applied during sample deposition. Substrate defects were isolated with a buffer Ta layer, and the texture of the IrMn and NiFe layers was improved with a 5-nm-thick Ta seed layer. The Ta<sub>2</sub>O<sub>5</sub>(2 nm)/Ta(4 nm) layer was formed during the natural oxidation of the Ta layer, which served to prevent oxidation in other layers of the structure.

Two series of the samples were fabricated under the same conditions: continuous thin films with an area of  $5 \times 5$  mm<sup>2</sup> [Fig. 1(a)] and patterned films with a Hall bridge of active area  $200 \times 200$  μm<sup>2</sup> [Fig. 1(b)]. Comparison of the continuous and patterned samples was important to avoid possible edge effects related to the magnetization as well as to current flow.

The patterned samples were designed by optical lithography. The sample preparation passed through three stages: creation of the sensor contact using photolithography, deposition of sensor contacts, and deposition of electrodes [Ta(5 nm)/Au(100 nm)]. To apply the current and register the transverse voltage, the patterned samples were connected to the printed circuit board (PCB) with West Bond 7476D paste. Then, the electrodes [Ta(5 nm)/Au(100 nm)] were connected to the tracks on the PCB with gold contacts using

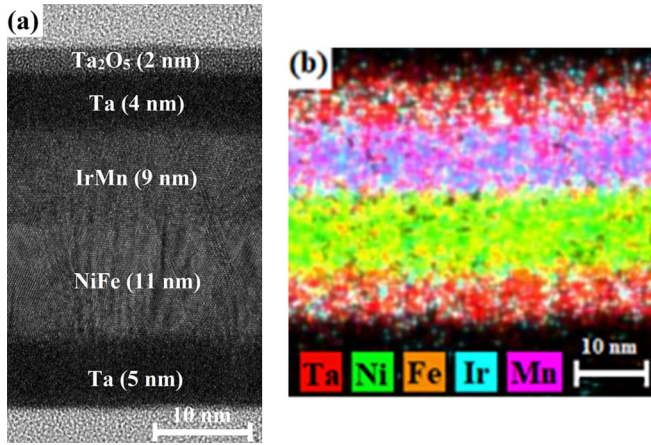


FIG. 2. (a) TEM image of a NiFe/IrMn cross section, (b) distribution of chemical elements Ta, Ni, Fe, Ir, and Mn shown in different colors, mapped by EDX technique in the NiFe/IrMn cross section.

microwelding for subsequent connection to a Keithley 6220 current source and a Keithley 2182A nanovoltmeter. In the upper part of Fig. 1(b), the two arrows indicate the direction of the applied magnetic field during structure deposition. This direction coincides with the easy axis of magnetization, direction of unidirectional anisotropy, and direction of exchange bias field.

External magnetic field was generated by electromagnet (Abbess Instruments) and it was measured by PCE-MFM 3000 in the vicinity of the sample.

Analysis of the cross section of samples was carried out using a high-resolution transmission electron microscope JEOL at an accelerating voltage of 200 kV [Fig. 2(a)] with equipment for energy-dispersive x-ray analysis (EDX) [Fig. 2(b)].

The x-ray-diffraction spectrum was obtained using a DRON-3M diffractometer using a copper tube ( $K_{\alpha 1}$  x rays with a wavelength of 1.54 Å) operating at 35 kV and 25 mA with a stability of 0.01%/8 h. The measurements were made in the range of angles  $2\theta = 35^\circ$ – $50^\circ$  with a step of  $0.2^\circ$ . The amplitude-normalized x-ray-diffraction spectrum of the NiFe/IrMn sample is shown in Fig. 3. The IrMn and NiFe layers have a cubic (111) texture. IrMn peaks correspond to

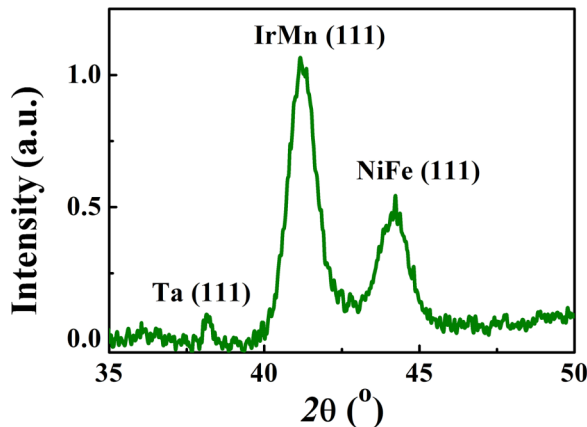


FIG. 3. Normalized XRD spectrum of NiFe/IrMn structure.

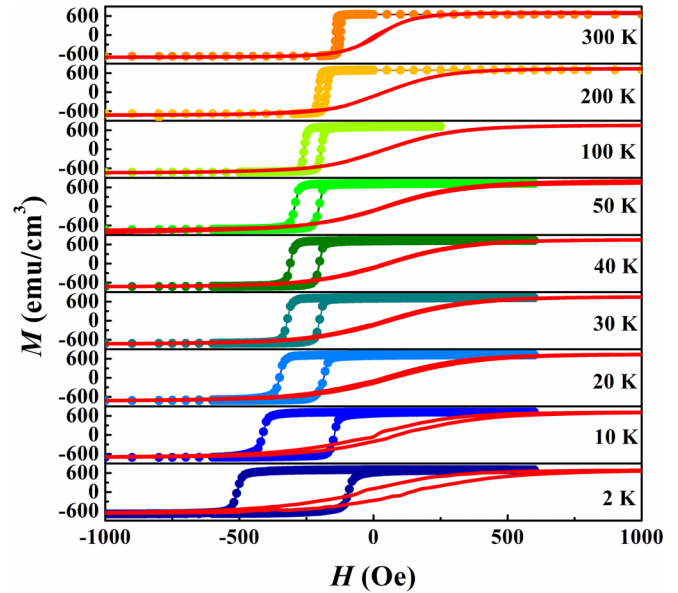


FIG. 4. Magnetic hysteresis loops recorded when field lies in plane along easy axis (colored points) and in out-of-plane orientation, when field is perpendicular to the sample (red line) at temperatures in the range of 2–300 K.

$2\theta = 41.3^\circ$ ; NiFe peaks correspond to  $2\theta = 44.2^\circ$ . As well, there is a small peak centered at  $38^\circ$ , which belongs to the (111) plane of the Ta layer. Estimation of the peak width using the Debye-Scherrer equation gives the thicknesses for NiFe and IrMn  $\sim 10$  nm, and for Ta  $\sim 4$  nm, which is comparable to the thicknesses of the layers determined by TEM.

The values of saturation magnetization of continuous thin films, their exchange bias, and coercive force were determined from the  $M$ – $H$  hysteresis loops recorded using a Quantum Design MPMS XL superconducting quantum interference device magnetometer in the temperature range from 2 to 300 K (Fig. 4). The saturation magnetization of  $M_S \approx 700$  emu/cm<sup>3</sup> corresponds to the literature data for pure Ni<sub>20</sub>Fe<sub>80</sub> permalloy [24]. Since the magnetization of the continuous sample is the same as in the patterned structure, one can neglect edge effects and scattering field.

In BLS experiments, the laser source with wavelength 532 nm, generated by Excelsior (Spectra Physics) EXLSR–532–200–CDRH, was used. It was shown in Ref. [26] that the magnetic properties and BLS spectra of NiFe/IrMn structures are the same in continuous films and in patterned samples. Laser spot of 25- $\mu$ m diameter was focused to the Hall cross center. Low power of laser irradiation of 20 mW excludes sample heating during experiments. Light penetration depth was 30–40 nm. This is well enough to penetrate through the all layers of heterostructure until substrate. Incidence angle was  $\alpha = 30^\circ$  in all experiments.

Light-scattering spectra were measured by the BLS method at room temperature in the Damon-Eshbach geometry, in which the direction of the magnetic moments in the sample  $M$  is perpendicular to the wave vector of the spin wave  $k_{sw}$  and perpendicular to the projection of the wave vector  $k$  of the incident light (Fig. 5).



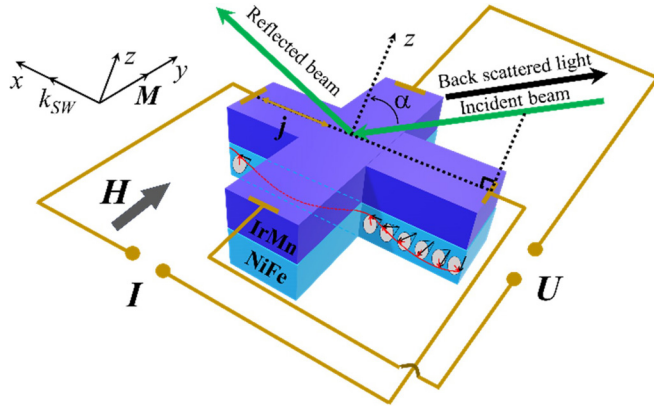


FIG. 5. Sketch of the BLS experiment in the Damon-Eshbach geometry. The  $\mathbf{k}_{\text{sw}}$  is the wave vector of the spin wave,  $\mathbf{M}$  is the direction of static magnetization caused by an external magnetic field lying in the plane of the sample,  $\alpha$  is angle between the incident light direction and the  $z$  axis,  $\mathbf{j}$  is current-density vector,  $U$  is voltage, and  $\mathbf{H}$  is external magnetic field. The spin wave caused by the precession of magnetic moments is shown on cross section by red line.

In-plane magnetic field in the range from  $-3$  to  $+3$  kOe was applied during experiments. Inversion of the field direction is equivalent to time inversion. As a result, Stokes and anti-Stokes peaks exchange their positions when the field is reoriented in the opposite direction. In our experiments, incidence angle  $30^\circ$  corresponds to projection of the light-wave vector to the film plane  $k_{x3} = 10 \times 10^{-4} \text{ cm}^{-1}$ . The BLS method is based on the inelastic scattering of photons by spin waves [27]. As a result of this process, a photon with frequency  $\omega_1$  and wave vector  $\mathbf{k}_1$  exchanges energy  $\Delta E_m$  and angular momentum  $\Delta p_m$  with the magnon. After that, phonon is reemitted. Based on the law of conservation of energy, the frequency and wave vector of the scattered photon ( $\omega_2$  and  $\mathbf{k}_2$ ) are expressed as

$$\hbar(\omega_1 - \omega_2) = \pm \Delta E_m, \quad (1)$$

$$\hbar(\mathbf{k}_1 - \mathbf{k}_2) = \pm \Delta p_m. \quad (2)$$

To explain the BLS spectra, magnon generation (Stokes scattering) and magnon annihilation (anti-Stokes scattering) should be considered. According to the selection rule, magnons with a wave vector  $\pm \mathbf{k}_{\text{sw}}$  equal to the projection of the incident light-wave vector  $\mathbf{k}_1$  will participate in light scattering. Scattering by a spin wave moving in the same direction as the light flux, when the vectors  $\mathbf{k}_{\text{sw}}$  and  $\mathbf{k}_1$  are codirected, decreases the photon frequency by the value  $\omega_{\text{sw}} = \omega_1 - \omega_2$ . In this case, the Stokes peak is observed in the scattering spectrum. When light scattered by a spin wave moving in the opposite direction to the light (vectors  $\mathbf{k}_{\text{sw}}$  and  $\mathbf{k}_1$  are antiparallel), the photon increases its energy and its frequency becomes  $\omega_{\text{sw}} = \omega_1 + \omega_2$ . In this case, the anti-Stokes peak will be observed in the scattering spectrum. Since laser emits photons with a strictly defined wavelength  $\omega_1$ , one can calculate the frequencies of spin waves with wave vectors  $-\mathbf{k}_{\text{sw}}$  and  $+\mathbf{k}_{\text{sw}}$ .

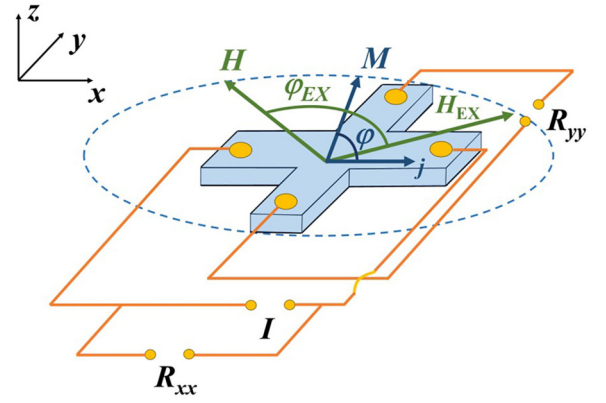


FIG. 6. Geometry of the experiments. Angle  $\varphi$  between the direction of electric current density  $\mathbf{j}$  and magnetization  $\mathbf{M}$ ; angle  $\varphi_{\text{EX}}$  between the magnetic field  $\mathbf{H}$  and the easy axis of magnetization ( $H_{\text{EX}}$ ).

### III. EXPERIMENTAL RESULTS AND DISCUSSION

#### A. Spin-torque effect on exchange-bias direction

Electrical measurements first were carried out on patterned samples to accurately determine the direction of the exchange-bias field in a patterned structure with a Hall bridge of  $4 \times 4 - \mu\text{m}^2$  sizes similarly with Ref. [16]. The change in the resistance of a thin magnetic film can be measured by the four-probe method at a constant electric current. In the coordinate system (Fig. 6), the resistance tensor can be written as [28]

$$R = \begin{bmatrix} R_{xx} & R_{xy} \\ R_{yx} & R_{yy} \end{bmatrix}. \quad (3)$$

All components correspond to in-plane electric currents. Diagonal components of this tensor  $R_{xx}$  and  $R_{yy}$  correspond to the longitudinal voltage measured along the current flow, while the off-diagonal components  $R_{xy}$  and  $R_{yx}$  correspond to transversal voltage [28]. Transverse voltage is planar Hall effect (PHE), while angular variations of longitudinal voltage correspond to anisotropic magnetoresistance (AMR). All resistance components of a thin film change with the angle  $\varphi$  between the direction of electric current density  $\mathbf{j}$  and magnetization  $\mathbf{M}$  [29]. At arbitrary angle  $\varphi$  longitudinal and transversal directions can be expressed as

$$R_{\text{AMR}} = R_{yy} + (R_{xx} - R_{yy})\cos^2\varphi, \quad (4)$$

$$R_{\text{PHE}} = (R_{xx} - R_{yy})\sin\varphi\cos\varphi. \quad (5)$$

The scheme of the AMR and PHE four-probe measurement is shown in Fig. 6.

According to the scheme in Fig. 6 we determine the values of resistances  $R_{xx}$  and  $R_{yy}$ . The angle  $\varphi$  cannot be measured directly, because direction of magnetization is unknown *a priori*. But, this angle  $\varphi$  can be calculated, since it depends on angle  $\varphi_{\text{EX}}$  manually set by goniometer between the magnetic field  $\mathbf{H}$  and the easy axis of magnetization. The easy axis is parallel to the direction of the exchange-bias field  $H_{\text{EX}}$  predetermined by sample growth in magnetic field. Dependence  $\varphi(\varphi_{\text{EX}})$  is usually calculated by minimization of magnetic energy  $E$

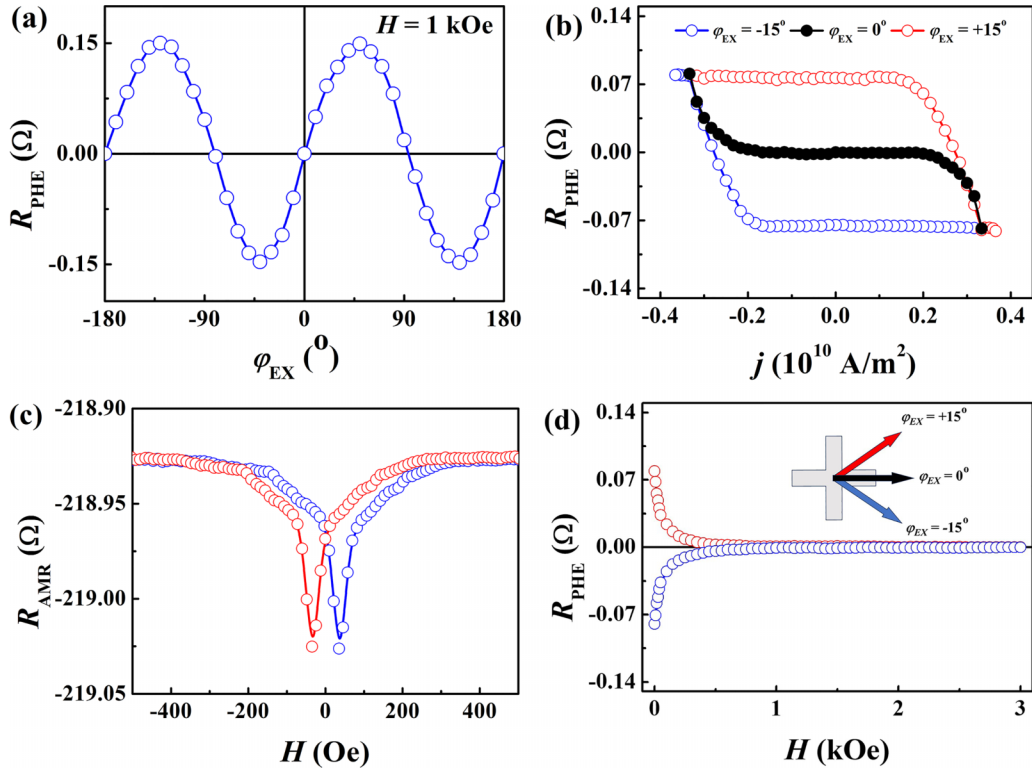


FIG. 7. (a) Angular dependence of resistance  $R_{\text{PHE}}(\varphi_{\text{EX}})$ . (b) Dependence of resistance  $R_{\text{PHE}}$  on current density  $j$  at  $\varphi_{\text{EX}} = 0^\circ$  (black symbols),  $\varphi_{\text{EX}} = -15^\circ$  (blue symbols), and  $\varphi_{\text{EX}} = +15^\circ$  (red symbols). (c) Field dependences of resistance  $R_{\text{AMR}}$  after preliminary applied current at  $\varphi_{\text{EX}} = -15^\circ$  (blue symbols),  $\varphi_{\text{EX}} = +15^\circ$  (red symbols); (d) field dependences of  $R_{\text{PHE}}$  measured after preliminary applied current at  $\varphi_{\text{EX}} = -15^\circ$  (blue symbols) and  $\varphi_{\text{EX}} = +15^\circ$  (red symbols). In the inset, scheme of exchange-bias direction  $\varphi_{\text{EX}}$  with respect to shoulder of the Hall cross is presented.

composed of Zeeman energy in magnetic field and anisotropy terms [30]:

$$E = K_{\text{U}} t_{\text{F}} \sin^2 \varphi - M_{\text{S}} t_{\text{F}} H \cos(\varphi - \varphi_{\text{EX}}) - M_{\text{S}} t_{\text{F}} H_{\text{EX}} \cos(\varphi), \quad (6)$$

where  $K_{\text{U}} = (1/2)H_{\text{U}}M_{\text{S}}$  is uniaxial anisotropy,  $H_{\text{U}}$  is uniaxial anisotropy field,  $M_{\text{S}}$  is saturation magnetization,  $H_{\text{EX}}$  is exchange bias field,  $t_{\text{F}}$  is thickness of ferromagnetic layer, and  $(\varphi - \varphi_{\text{EX}})$  is angle between magnetization  $\mathbf{M}$  and magnetic field  $\mathbf{H}$  (Fig. 6).

In thin films NiFe/IrMn [31–34] and NiFe/FeMn [35–39], the condition  $H_{\text{U}} \ll H_{\text{EX}}$  is fulfilled, and dependence  $\varphi(\varphi_{\text{EX}})$  can be expressed in the analytical form:

$$\cos \varphi \sim \frac{H_{\text{EX}} + H \cos \varphi_{\text{EX}}}{\sqrt{H^2 \sin^2 \varphi_{\text{EX}} + (H_{\text{EX}} + H \cos \varphi_{\text{EX}})^2}}, \quad (7)$$

$$\sin \varphi \sim \frac{H \sin \varphi_{\text{EX}}}{\sqrt{H^2 \sin^2 \varphi_{\text{EX}} + (H_{\text{EX}} + H \cos \varphi_{\text{EX}})^2}}. \quad (8)$$

Substitution of experimentally determined resistance components  $R_{xx}$  and  $R_{yy}$  and calculated  $\varphi$  to Eq. (5) at each fixed  $\varphi_{\text{EX}}$  results in angular dependence  $R_{\text{PHE}}(\varphi_{\text{EX}})$ . This dependence was plotted at constant current 1 mA in magnetic field 1 kOe [Fig. 7(a)]. In the external magnetic field  $H$  parallel or perpendicular to the direction of the exchange-bias field  $H_{\text{EX}}$ , resistance is zero,  $R_{\text{PHE}} = 0$ . At the angle  $\varphi_{\text{EX}} = 45^\circ$ , resistance  $R_{\text{PHE}}$  reaches a maximum value of 0.15  $\Omega$ .

In our samples, we verified the electrical control over exchange bias induced by spin-orbit torque (SOT) reported in Ref. [16]. In Fig. 7(b), change in resistance  $R_{\text{PHE}}$  as a function of in-plane current amplitude  $j$  in an IrMn(9 nm)/NiFe(11 nm) sample is presented. Rectangular current impulse duration was 50  $\mu\text{s}$ . Initial direction of magnetization corresponds to  $\varphi_{\text{EX}} = 0^\circ$  direction (black symbols). Increase of  $j$  (blue symbols) does not affect  $R_{\text{PHE}}$  until  $j = +0.2 \times 10^{10} \text{ A/m}^2$ , but the resistance  $R_{\text{PHE}}$  decreases down at  $j > +0.35 \times 10^{10} \text{ A/m}^2$  until saturation value,  $R_{\text{PHE}} = -0.08 \Omega$ . Saturation of the Hall resistance  $R_{\text{PHE}} = -0.08 \Omega$  corresponds to the exchange-bias direction,  $\varphi_{\text{EX}} = -15^\circ$ . In Ref. [16], at  $\varphi_{\text{EX}} = -15^\circ$  value  $R_{\text{PHE}}$  was  $-0.14 \Omega$ , because the thickness of the Hall cross was larger in our experiments. Decrease of current down to  $j \sim -0.2 \times 10^{10} \text{ A/m}^2$  causes increase in  $R_{\text{PHE}}$  corresponding to change of exchange-bias direction from  $\varphi_{\text{EX}} = -15^\circ$  to  $\varphi_{\text{EX}} = +15^\circ$  at  $j = -0.35 \times 10^{10} \text{ A/m}^2$  and  $R_{\text{PHE}} = +0.08 \Omega$ . Similar variations of  $R_{\text{PHE}}$  and  $\varphi_{\text{EX}}$  were observed if initially negative current  $j < 0$  was applied (red symbols). Dependence of  $R_{\text{AMR}}(H)$  [Fig. 7(c)] shifts if sign of  $\varphi_{\text{EX}}$  alternates [Fig. 7(c)]. This indicates residual changes initiated by electric current in interface layer, where exchange bias is formed.

Dependence of resistance  $R_{\text{PHE}}(H)$  on the field directed along the  $x$  axis was recorded [Fig. 7(d)]. At the beginning current density  $j = -0.35 \times 10^{10} \text{ A/m}^2$  was settled with positive  $R_{\text{PHE}} = +0.08 \Omega$  corresponding to  $\varphi_{\text{EX}} = +15^\circ$ . Increase of magnetic field along the  $x$  axis causes decrease

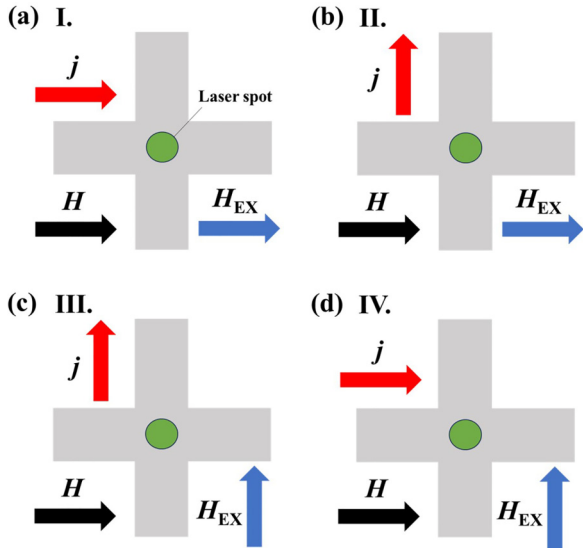


FIG. 8. Schemes of four types of BLS experiments with different mutual orientations of  $\mathbf{j}$ ,  $\mathbf{H}_{\text{EX}}$ , and  $\mathbf{H}$  vectors NiFe/IrMn samples.

of  $R_{\text{PHE}}$  down to zero, indicating magnetization alignment along the  $x$  axis. The same rotation of exchange bias with increase of field was observed at the initial negative resistance,  $R_{\text{PHE}} = -0.08 \Omega$  [Fig. 7(d)]. Restoration of the initial  $R_{\text{PHE}}$  value after removing the field indicates presence of the bias field directed along  $\varphi_{\text{EX}} = +15^\circ$  angle. This field appears due to IrMn layer. Thus, in our experiments direction of exchange bias is controlled by SOT accompanying electric current.

### B. Spin-torque effect on Brillouin light scattering

In the following series of experiments, we demonstrate that BLS spectra are affected by switching of exchange bias under SOT action in patterned samples NiFe/IrMn. For that purpose directions of current  $\mathbf{j}$  and magnetization  $\mathbf{M}$  were changed. We performed four types of experiments at different mutual orientations of  $\mathbf{j}$ ,  $\mathbf{M}$ , and  $\mathbf{H}$  vectors in BLS spectrometer [Figs. 8(a)–8(d)]. In-plane external magnetic field  $H$  was perpendicular to the light incidence plane. First, BLS spectrum in magnetic field  $H = +3$  kOe at zero electric current was recorded [Fig. 9(a)]. This reference spectrum recorded in absence of current was used to compare amplitude, frequency, and linewidth in other spectra for Stokes and anti-Stokes lines. Series of the BLS spectra recorded for configuration I at different current densities are presented in Figs. S1(a)–S1(d) of Supplemental Material [40].

Upon application of electric current  $j = +0.35 \times 10^{10}$  A/m<sup>2</sup>, in configuration I [Fig. 8(a)], when current, field, and magnetization are collinear, amplitude of the Stokes line increases, while amplitude of the anti-Stokes line decreases [Fig. 9(b)]. Frequency of maximum  $\sim 20$ –21 GHz does not change. In contrast, alteration of the current direction from  $j = +0.35 \times 10^{10}$  to  $j = -0.35 \times 10^{10}$  A/m<sup>2</sup> increases anti-Stokes line amplitude and decreases Stokes line amplitude [Fig. 9(c)]. Thus, SOT-driven magnetization redistributes asymmetry of the Stokes and anti-Stokes lines. In our previous work, the effect of magnetic field inversion on

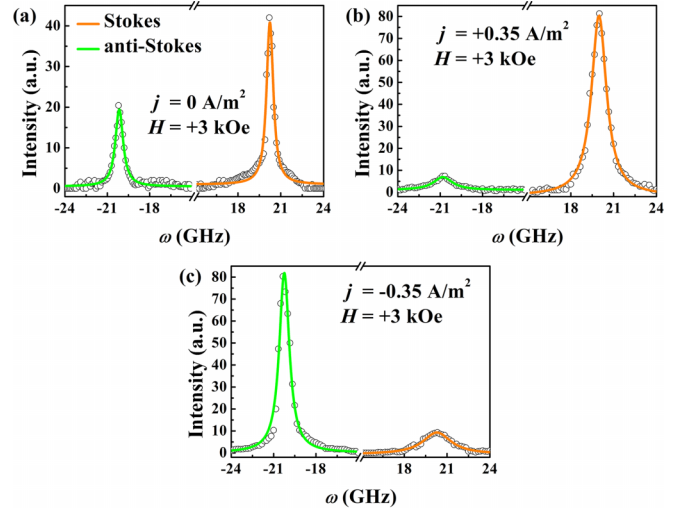


FIG. 9. BLS spectra (a) at zero current, (b) under current  $j = +0.35 \times 10^{10}$  A/m<sup>2</sup> directed along field, and (c) under current  $j = -0.35 \times 10^{10}$  A/m<sup>2</sup> directed opposite to field. All BLS spectra were recorded accordingly with scheme presented in Fig. 8(a).

asymmetry of the Stokes and anti-Stokes lines in NiFe/IrMn structure was reported [41].

Variation of current density  $j$  in the range from  $-0.2 \times 10^{10}$  to  $+0.2 \times 10^{10}$  A/m<sup>2</sup> in configuration II [Fig. 8(b)] does not change BLS spectrum [Figs. 10(a) and 10(b)]. Increase in current density from  $+0.2 \times 10^{10}$  to  $+0.35 \times 10^{10}$  A/m<sup>2</sup> gives rise to Stokes line, while anti-Stokes line remains constant [Figs. 10(c) and 10(e)]. Increase in  $j$  from  $-0.2 \times 10^{10}$  to  $-0.25 \times 10^{10}$  A/m<sup>2</sup> gradually equalizes Stokes and anti-Stokes lines due to the growth of the anti-Stokes line [Fig. 10(d)]. Following increase in absolute value of current density up to  $-0.35 \times 10^{10}$  A/m<sup>2</sup> gives rise to anti-Stokes line, while Stokes line remains constant [Fig. 10(f)]. Thus, threshold value of current density exists. Series of BLS spectra at multiple  $j$  values for configuration II are presented in Figs. S2(a)–S2(d) of Supplemental Material [40].

At magnetization perpendicular to magnetic field, accordingly with schemes III and IV [Figs. 8(c) and 8(d)], BLS spectra remain constant independently of current density from  $-0.35 \times 10^{10}$  to  $-0.35 \times 10^{10}$  A/m<sup>2</sup> [Figs. 11(a)–11(d)]. Series of BLS spectra for others  $j$  values in the configurations III and IV are presented in Figs. S3(a)–S3(d) and Figs. S4(a)–S4(d), respectively, of Supplemental Material [40].

Although electric current changes amplitudes of Stokes and anti-Stokes lines, widths  $\sim 0.5$ –1.5 GHz and positions  $\pm 20$ –21 GHz of these lines remain constant.

Asymmetry of BLS spectrum was characterized as a ratio of Stokes intensity  $I_S$  to anti-Stokes intensity  $I_{AS}$ . Dependence of this ratio  $I_S/I_{AS}$  on current density for different configurations I – IV (Fig. 8) at external fields +3 and –3 kOe are presented in Fig. 12.

Increasing and decreasing behavior of the  $I_S/I_{AS}(j)$  depends on current direction [Figs. 12(a) and 12(b)]. In configuration I, we observed gradual exponential-like dependences  $I_S/I_{AS}(j)$  [Fig. 12(a)], while in configuration II, sharp drops of the  $I_S/I_{AS}(j)$  dependences were observed. The possible reason of that is perpendicularity of bias field and current

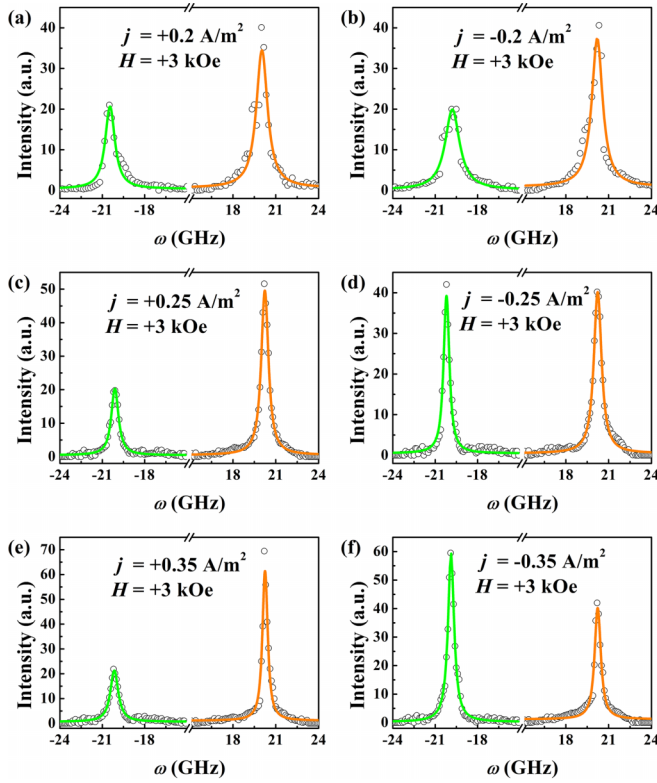


FIG. 10. BLS spectra recorded at current densities  $j = +0.2 \times 10^{10}$  A/m<sup>2</sup> (a),  $-0.2 \times 10^{10}$  A/m<sup>2</sup> (b),  $+0.25 \times 10^{10}$  A/m<sup>2</sup> (c),  $-0.25 \times 10^{10}$  A/m<sup>2</sup> (d),  $+0.35 \times 10^{10}$  A/m<sup>2</sup> (e), and  $-0.35 \times 10^{10}$  A/m<sup>2</sup> (f). All spectra were recorded accordingly with scheme **II** in Fig. 8(b).

in configuration **II**. This probably requires critical value of current to change bias direction. Dependences  $I_S/I_{AS}(j)$  in Fig. 12(b) are similar to dependence  $R_{PHE}(j)$  in Fig. 7(b). This fact confirms reliability of BLS probe in configuration **II**. In configurations **III** and **IV** the current density does not change the intensities of the Stokes and anti-Stokes lines [Fig. 12(c)], because magnetic field is directed along the hard axis.

Intensities of the Stokes and anti-Stokes lines depend on geometry of scattering and incident light polarization. In our experiments, light is polarized in incident plane (*p*-polarized light). In these conditions, Stokes and anti-Stokes intensities can be expressed as [42]

$$\begin{aligned} I_S &= |(m_y E_x - m_x E_y)|^2, \\ I_{AS} &= |(m_y^* E_x - m_x^* E_y)|^2, \end{aligned} \quad (9)$$

where  $m_x$ ,  $m_y$ ,  $E_x$ , and  $E_y$  are complex amplitudes of components of dynamical magnetization and electric field, respectively. Equation (9) can explain asymmetry of Stokes and anti-Stokes lines. Relative contributions of  $m_x$  and  $m_y$  components determine ratio  $I_S/I_{AS}$

$$\frac{I_S}{I_{AS}} = \frac{\left|1 - \left(\frac{m_x}{m_y}\right)\left(\frac{E_y}{E_x}\right)\right|^2}{\left|1 - \left(\frac{m_x}{m_y}\right)^* \left(\frac{E_y}{E_x}\right)\right|^2}, \quad (10)$$

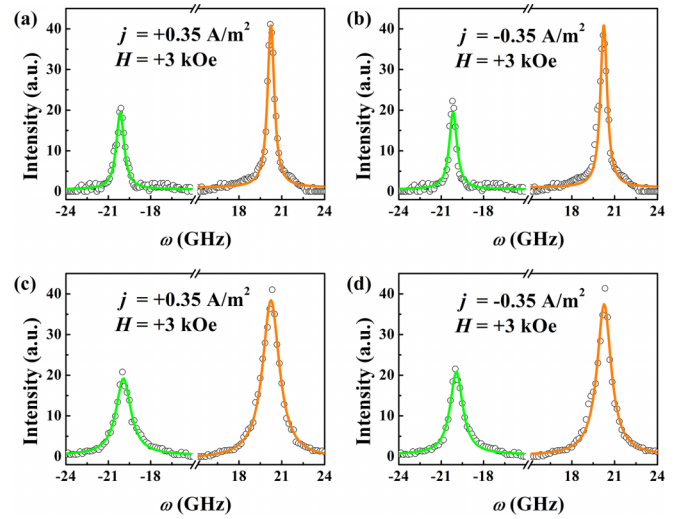


FIG. 11. BLS spectra at current densities  $j = +0.35 \times 10^{10}$  A/m<sup>2</sup> (a) and  $-0.35 \times 10^{10}$  A/m<sup>2</sup> (b) were recorded at orientations of current, field, and magnetization corresponding to Fig. 8(c). BLS spectra at current densities  $j = +0.35 \times 10^{10}$  A/m<sup>2</sup> (c) and  $-0.35 \times 10^{10}$  A/m<sup>2</sup> (d) were recorded accordingly with Fig. 8(d).

where the estimated ratio  $E_x/E_y \sim 0.58$  corresponds to the light polarization.

In thin film of thickness  $d$ , wave mode with wave vector  $k$  corresponds to equations determining ferromagnetic resonance. In this case ratio  $|m_x/m_y|$  can be expressed as [42,43]

$$\frac{|m_x|}{|m_y|} = \frac{\sqrt{H_{\text{EFF}} + 4\pi M_S - 2\pi M_S k d}}{\sqrt{H_{\text{EFF}} + 2\pi M_S k d}}. \quad (11)$$

We introduced to Eq. (11) the term describing effective field of SOT,  $H_{\text{EFF}} = \pm H \pm \hbar \frac{\xi}{2eM_S} t_F$ , accordingly with Ref. [44]. In this formula,  $\hbar$  is Planck constant,  $e$  is electron charge, and  $\xi$  is SOT efficiency constant. Sign of SOT effective field as well as sign of the external field  $H$  depends on experiment configuration in Fig. 8. Substitution of formula (11) to expression (10) allowed us to approximate  $I_S/I_{AS}(j)$  dependences [Figs. 12(a) and 12(b)]. We determined SOT efficiency  $\xi = 0.8$  in configurations **I** and **II**. These values are similar to ones determined in Ref. [44].

Thus, we found the effect of the current density on the intensities of the Stokes and anti-Stokes lines in the BLS spectra. This effect is provided by SOT effect on the exchange-bias field direction in IrMn layer. This effect is equivalent to the change in the reflected light color. The thin film NiFe/IrMn plays the role of an electrically controlled mirror. We also demonstrate the possibility of electrical control over the direction of spin waves and electrical manipulation by Stokes and anti-Stokes intensities. Our findings pave the way for the creation of electro-optical device that tunes the light frequency.

We have compared dependences of BLS spectra on incidence angle  $\alpha$  corresponding to wave vector  $k$  and magnetic field in continuous and patterned samples [Figs. 13(a) and 13(b)]. These dependences were identical.

Dispersion function is symmetrical in respect to wave vector  $k$  in continuous and patterned samples, NiFe/IrMn



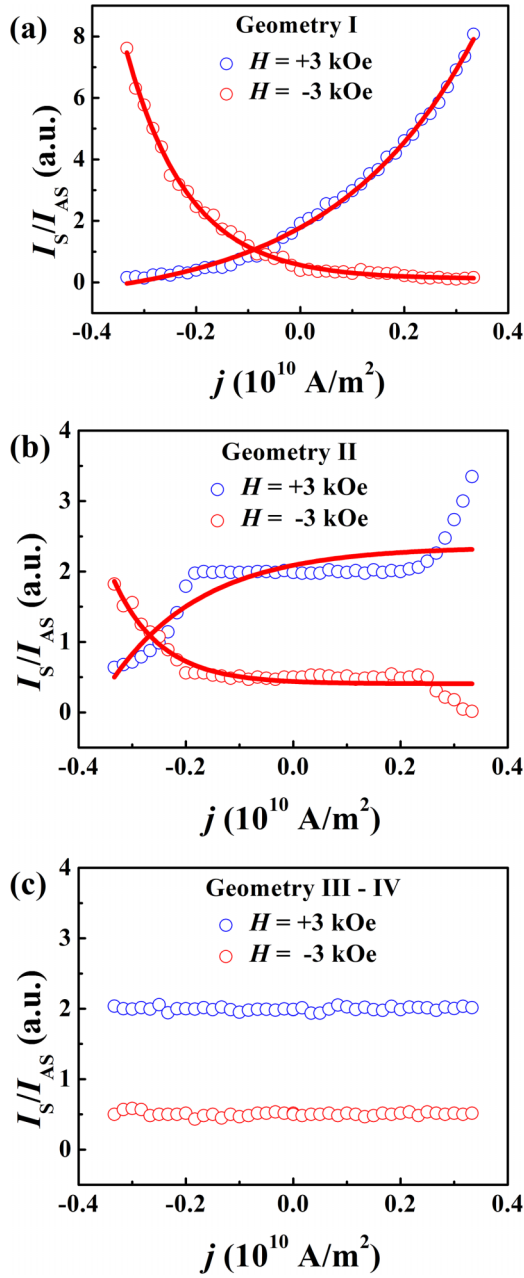


FIG. 12. Dependences of ratio  $I_S/I_{AS}$  of Stokes intensity  $I_S$  to anti-Stokes intensity  $I_{AS}$  on current density for three different experimental configurations **I** – **III** listed in Fig. 8 in magnetic fields  $H = +3$  and  $-3$  kOe. Experiment of **I** type [Fig. 8(a)], **II** type [Fig. 8(b)], and **III** type [Fig. 8(c)]. Experiments of **III** and **IV** are identical to each other. Solid lines in (a), (b) are approximations by Eqs. (9)–(11).

[Fig. 13(a)]. Thus, patterning does not affect spin-wave propagation. The BLS spectra with varying angle of incidence beam  $\alpha$  are presented in the Supplemental Material in Fig. S5 [40]. The BLS spectra recorded at different external magnetic fields are shown in the Supplemental Material in Fig. S6 [40].

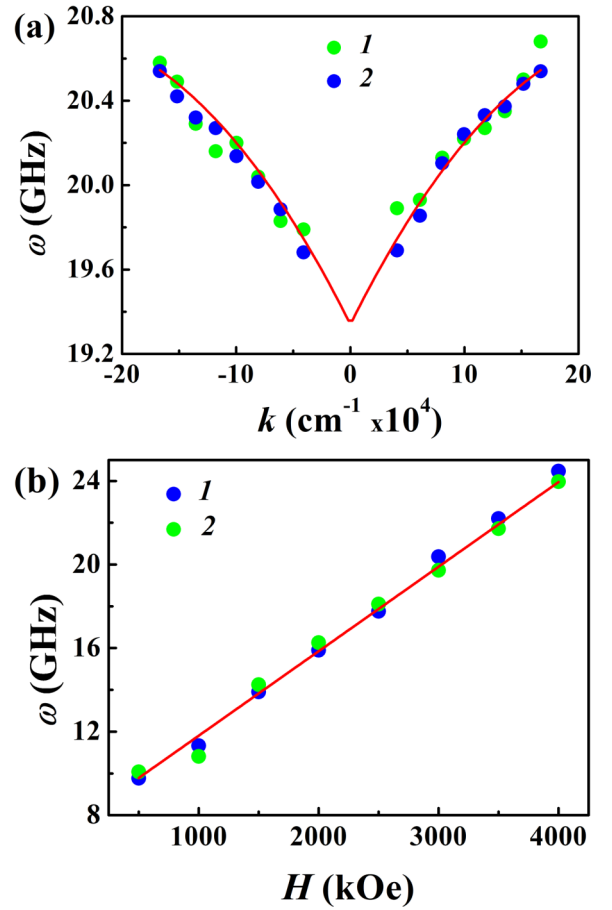


FIG. 13. (a) Dependence of Stokes and anti-Stokes maxima frequency on wave number  $k$ . Solid line is approximations by Eq. (12). (b) Dependences of Stokes and anti-Stokes maxima frequencies on magnetic field. Solid line is approximations by Eq. (13). 1: continuous samples; 2: patterned samples.

In the experimental geometry, corresponding to Fig. 8(a), frequency of spin wave can be expressed as [24,41]

$$\left(\frac{\omega}{\gamma}\right)^2 = \left[ H + H_U + H_{RA} + 2\pi M_S k_T F + Dk^2 + \frac{H_W}{\left(\frac{H_W}{H_{EX}}\right) + 1} \right] \times \left[ H + 4\pi M_{EFF} + H_U + H_{RA} - 2\pi M_S k_T F + Dk^2 + \frac{H_W}{\left(\frac{H_W}{H_{EX}}\right) + 1} \right], \quad (12)$$

where  $\gamma$  is the gyromagnetic ratio (in NiFe  $\gamma = 17.6$  GHz/kOe [24]),  $H_U$  is uniaxial anisotropy field,  $H_{RA}$  is field of rotation anisotropy,  $M_S \approx 700$  emu/cm<sup>3</sup> is saturation magnetization in NiFe [24],  $D \approx 2 \times 10^{-9}$  Oe cm<sup>2</sup> is exchange stiffness [45], and  $H_W$  is domain-wall field. Approximation of dispersion curves  $\omega(k)$  by Eq. (12) [see solid line in Fig. 13(a)] results in the following parameters:  $H_U = 45$  Oe,  $H_{RA} = 420$  Oe,



and  $H_{\text{EX}} = 120$  Oe. Domain-wall field  $H_{\text{W}} = 1$  kOe is similar with one in structure NiFe/IrMn in Ref. [46].

Additionally, we approximated field dependence of BLS frequency in the same configuration. If one neglects field of single-axis anisotropy, dependence  $\omega(H)$  can be expressed as [47]

$$\omega = \frac{\gamma}{2\pi} \left( \left( H + H_{\text{EX}} + 2\pi M_{\text{S}} k_{\text{T}} \sin^2 \alpha + \frac{2Dk^2}{M_{\text{S}}} \right) \times \left( H + H_{\text{EX}} + 4\pi M_{\text{EFF}} - 2\pi M_{\text{S}} k_{\text{T}} + \frac{2Dk^2}{M_{\text{S}}} \right) \right)^{1/2}. \quad (13)$$

Approximation of  $\omega(H)$  dependence is shown in Fig. 13(b). We used the following parameters:  $\gamma = 17.6$  GHz/kOe,  $M_{\text{S}} \approx 700$  emu/cm<sup>3</sup>,  $k = 117990$  cm<sup>-1</sup> ( $\alpha = 30^\circ$ ), and  $D \approx 2 \times 10^{-9}$  Oe cm<sup>2</sup>. This approximation results in  $H_{\text{EX}} = 116$  Oe and  $4\pi M_{\text{EFF}} = 4127$  Oe. These are reasonable parameters standard for NiFe/IrMn structures [47]. This confirms reliability of the data obtained.

#### IV. CONCLUSIONS

The influence of the electric current passing in the IrMn antiferromagnetic layer on the BLS spectra of the adjacent NiFe ferromagnetic layer in NiFe/IrMn structures was found. The application of an electric current along the magnetic field

leads to the suppression of the anti-Stokes component of the BLS spectrum, while application of electric current in the opposite direction against the field leads to the disappearance of the Stokes component.

Simultaneously with the change in the BLS spectra, there is a change in the direction of the exchange-bias field, which was previously discovered in the works of other authors and detected by the Hall voltage. The change in the direction of the exchange bias is caused by the action of spin-orbit torque generated in the IrMn layer near the NiFe/IrMn interface. The spin-orbit torque controls the exchange bias and the corresponding unidirectional anisotropy field in the IrMn antiferromagnetic layer. SOT-induced change in the exchange bias in turn creates an asymmetry in the amplitudes of the forward and backward spin waves in the BLS spectra of the NiFe ferromagnet.

The obtained results can be used for ultrafast magneto-optical switching of light frequency reflected from a ferromagnet by electric current and for the creation of current-controlled antiferromagnetic spintronics devices.

#### ACKNOWLEDGMENT

The work was supported by the thematic map of the Federal Research Center for Problems of Chemical Physics and Medical Chemistry of the Russian Academy of Sciences Grant No. FFSG-2024-0009.

- 
- [1] T. Jungwirth, X. Marti, P. Wadley, and J. Wunderlich, *Nat. Nanotechnol.* **11**, 231 (2016).
- [2] O. Gomonay, T. Jungwirth, and J. Sinova, *Phys. Status Solidi RRL* **11**, 1700022 (2017).
- [3] H. Yan, Z. Feng, P. Qin, X. Zhou, H. Guo, X. Wang, H. Chen, X. Zhang, H. Wu, C. Jiang, and Z. Liu, *Adv. Mater.* **32**, 1905603 (2020).
- [4] D. Xiong, Y. Jiang, K. Shi, A. Du, Y. Yao, Z. Guo, D. Zhu, K. Cao, S. Peng, W. Cai, D. Zhu, and W. Zhao, *Fundam. Res.* **2**, 522 (2022).
- [5] V. Baltz, A. Manchon, M. Tsoi, T. Moriyama, T. Ono, and Y. Tserkovnyak, *Rev. Mod. Phys.* **90**, 015005 (2018).
- [6] C. Zhou, Y. P. Liu, Z. Wang, S. J. Ma, M. W. Jia, R. Q. Wu, L. Zhou, W. Zhang, M. K. Liu, Y. Z. Wu, and J. Qi, *Phys. Rev. Lett.* **121**, 086801 (2018).
- [7] H. Qiu, L. Zhou, C. Zhang, J. Wu, Y. Tian, S. Cheng, S. Mi, H. Zhao, Q. Zhang, D. Wu, B. Jin, J. Chen, and P. Wu, *Nat. Phys.* **17**, 388 (2021).
- [8] S. Shim, M. Menhaen, J. Sklenar, J. Oh, J. Gibbons, H. Saglam, A. Hoffmann, S. S.-L. Zhang, and N. Mason, *Phys. Rev. X* **12**, 021069 (2022).
- [9] A. Hoffmann, *IEEE Trans. Magn.* **49**, 5172 (2013).
- [10] J. B. S. Mendes, R. O. Cunha, O. A. Santos, P. R. T. Ribeiro, F. L. A. Machado, R. L. Rodriguez-Suarez, A. Azevedo, and S. M. Resende, *Phys. Rev. B* **89**, 140406(R) (2014).
- [11] L. Huang, Y. Zhou, H. Qiu, H. Bai, C. Chen, W. Yu, L. Liao, T. Guo, F. Pan, B. Jin, and C. Song, *Adv. Mater.* **34**, 2205988 (2022).
- [12] P. Gambardella and I. M. Miron, *Philos. Trans. R. Soc. A* **369**, 3175 (2011).
- [13] R. Ramaswamy, J. M. Lee, K. Cai, and H. Yang, *Appl. Phys. Rev.* **5**, 031107 (2018).
- [14] Q. Shao, P. Li, L. Liu, H. Yang, S. Fukami, A. Razavi, H. Wu, K. Wang, F. Freimuth, Y. Mokrousov, M. D. Stiles, S. Emori, A. Hoffmann, J. Akerman, K. Roy, J.-P. Wang, S.-H. Yang, K. Garello, and W. Zhang, *IEEE Trans. Magn.* **57**, 800439 (2021).
- [15] C. Song, R. Zhang, L. Liao, Y. Zhou, X. Zhou, R. Chen, Y. You, X. Chen, and F. Pan, *Prog. Mater. Sci.* **118**, 100761 (2021).
- [16] J. Kang, J. Ryu, J.-G. Choi, T. Lee, J. Park, S. Lee, H. Jang, Y. S. Jung, K.-J. Kim, and B.-G. Park, *Nat. Commun.* **12**, 6420 (2021).
- [17] J. Zelezny, P. Wadley, K. Olejnik, A. Hoffmann, and H. Ohno, *Nat. Phys.* **14**, 220 (2018).
- [18] M. Dunz, T. Matalla-Wagner, and M. Meinert, *Phys. Rev. Res.* **2**, 013347 (2020).
- [19] H. Wang, J. Finley, P. Zhang, J. Han, J. T. Hou, and L. Liu, *Phys. Rev. Appl.* **11**, 044070 (2019).
- [20] R. L. Stamps, *J. Phys. D : Appl. Phys.* **33**, R247 (2000).
- [21] K. O'Grady, L. E. Fernandez-Outon, and G. Vallejjo-Fernandez, *J. Magn. Magn. Mater.* **322**, 883 (2010).
- [22] P. Miltenyi, M. Gruyters, G. Guntherodt, J. Nogués, and I. K. Schuller, *Phys. Rev. B* **59**, 3333 (1999).
- [23] C. Mathieu, M. Bauer, B. Hillebrands, J. Fassbender, G. Guntherodt, R. Jungblut, J. Kohlhepp, and A. Reinders, *J. Appl. Phys.* **83**, 2863 (1998).
- [24] R. L. Rodriguez-Suarez, A. B. Oliveira, F. Estrada, D. S. Maior, M. Arana, O. A. Santos, A. Azevedo, and S. M. Rezende, *J. Appl. Phys.* **123**, 043901 (2018).

- [25] V. Tshitoyan, C. Ciccarelli, A. P. Mihai, M. Ali, A. C. Irvine, T. A. Moore, T. Jungwirth, and A. J. Ferguson, *Phys. Rev. B* **92**, 214406 (2015).
- [26] J. F. Cochran, *J. Magn. Magn. Mater.* **212**, 40 (2000).
- [27] E. R. Moog, S. D. Bader, and J. Zak, *Appl. Phys. Lett.* **56**, 2687 (1990).
- [28] L. Jogschies, D. Klaas, R. Kruppe, J. Rittinger, P. Taptimthong, A. Wienecke, L. Rissing, and M. C. Wurz, *Sensors* **15**, 28665 (2015).
- [29] A. D. Henriksen, B. T. Dalslet, D. H. Skieller, K. H. Lee, F. Okkels, and M. F. Hansen, *Appl. Phys. Lett.* **97**, 013507 (2010).
- [30] T. Q. Hung, S. Oh, B. Sinha, J.-R. Jeong, D.-Y. Kim, and C. G. Kim, *J. Appl. Phys.* **107**, 09E715 (2010).
- [31] A. Talantsev, M. Bakhmetiev, and R. Morgunov, *J. Phys. D: Appl. Phys.* **55**, 315002 (2022).
- [32] S. K. Mishra, F. Radu, S. Valencia, D. Schmitz, E. Schierle, H. A. Dürr, and W. Eberhardt, *Phys. Rev. B* **81**, 212404 (2010).
- [33] R. B. da Silva, M. A. Correa, E. F. Silva, T. J. A. Mori, R. D. Della Pace, R. Dutra, A. D. C. Viegas, F. Bohn, and R. L. Sommer, *Appl. Phys. Lett.* **104**, 102405 (2014).
- [34] R. B. da Silva, E. F. Silva, T. J. A. Mori, R. D. Della Pace, R. Dutra, M. A. Corrêa, F. Bohn, and R. L. Sommer, *J. Magn. Magn. Mater.* **394**, 87 (2015).
- [35] M. Gloanec, S. Rioual, B. Lescop, R. Zuberek, R. Szymczak, P. Aleshkevych, and B. Rouvellou, *Phys. Rev. B* **82**, 144433 (2010).
- [36] V. P. Nascimento, E. C. Passamani, A. Biondo, V. B. Nunes, and E. B. Saitovitch, *Appl. Surf. Sci.* **253**, 6248 (2007).
- [37] Z. B. Guo, Y. H. Wu, J. J. Qiu, B. Y. Zong, and G. C. Han, *Phys. Rev. B* **78**, 184413 (2008).
- [38] Y. Wang, B. Dai, B. Huang, Y. Ren, J. Xu, Z. Wang, S. Tan, and J. Ni, *J. Mater. Sci.: Mater. Electron.* **27**, 3778 (2016).
- [39] M. Donolato, B. T. Dalslet, C. D. Damsgaard, K. Gunnarsson, C. S. Jacobsen, P. Svedlindh, and M. F. Hansen, *J. Appl. Phys.* **109**, 064511 (2011).
- [40] See Supplemental Material at <http://link.aps.org/supplemental/10.1103/PhysRevB.109.024433> for the series of the BLS spectra recorded for configurations **I**, **II**, **III**, and **IV** at different current densities; the BLS spectra with varying angle of incidence beam  $\alpha$ ; the BLS spectra recorded at different external magnetic fields.
- [41] M. Bakhmetiev, A. Talantsev, A. Sadovnikov, and R. Morgunov, *J. Phys. D: Appl. Phys.* **55**, 105001 (2022).
- [42] R. Ziveri, P. Vavassori, L. Giovannini, F. Nizzoli, E. E. Fullerton, M. Grimsditch, and V. Metlushko, *Phys. Rev. B* **65**, 165406 (2002).
- [43] M. Grimsditch, S. Kumar, and E. E. Fullerton, *Phys. Rev. B* **54**, 3385 (1996).
- [44] W. Skowronski, M. Cecot, J. Kanak, S. Zietek, T. Stobiecki, L. Yao, S. Dijken, T. Nozaki, K. Yakushiji, and S. Yuasa, *Appl. Phys. Lett.* **109**, 062407 (2016).
- [45] S. M. Rezende, C. Chesman, M. A. Lucena, A. Azevedo, and F. M. Aguiar, *J. Appl. Phys.* **84**, 958 (1998).
- [46] M. A. Sousa, F. Pelegrini, W. Alayo, J. Quispe-Marcatoma, and E. Baggio-Saitovitch, *Physica B: Condens. Matter* **450**, 167 (2014).
- [47] A. Haldar, C. Banerjee, P. Laha, and A. Baman, *J. Appl. Phys.* **115**, 133901 (2014).